ASME Journal of Biomechanical Engineering
Online journal at:
https://asmedigitalcollection.asme.org/biomechanical

Constitutive Modeling of Mouse Arteries Suggests Changes in Directional Coupling and Extracellular Matrix Remodeling That Depend on Artery Type, Age, Sex, and Elastin Amounts

Keshav A. Kailash
Biomedical Engineering,
Washington University,
St. Louis, MO 63130

Jie Z. Hawes
Mechanical Engineering and Materials Science,
Washington University,
St. Louis, MO 63130

Austin J. Cocciolone
Mechanical Engineering and Materials Science,
Washington University,
St. Louis, MO 63130

Matthew R. Bersi
Mechanical Engineering and Materials Science,
Washington University,
St. Louis, MO 63130

Robert P. Mecham
Cell Biology and Physiology,
Washington University,
St. Louis, MO 63130

Jessica E. Wagenseil[1]
Mechanical Engineering and Materials Science,
Washington University,
One Brookings Dr., MSC 1185-208-125,
St. Louis, MO 63130
e-mail: jessica.wagenseil@wustl.edu

Arterial stiffening occurs during natural aging, is associated with an increased risk of adverse cardiovascular events, and can follow different timelines in males and females. One mechanism of arterial stiffening includes remodeling of the extracellular matrix (ECM), which alters the wall material properties. We used elastin haploinsufficient ($Eln^{+/-}$) and wildtype ($Eln^{+/+}$) mice to investigate how material properties of two different arteries (ascending aorta and carotid artery) change with age, sex, and ECM composition. We used a constitutive model by Dong and Sun that is based on the Holzapfel–Gasser–Ogden (HGO) type, but does not require a discrete number of fibrous ECM families and allows varied deformation coupling. We find that the amount of deformation coupling for the best fit model depends on the artery type. We also find that remodeling to maintain homeostatic (i.e., young, wildtype) values of biomechanical parameters with age, sex, and ECM composition depends on the artery type, with ascending aorta being more adaptable than carotid artery. Fitted material constants indicate sex-dependent remodeling that may be important for determining the time course of arterial stiffening in males and females. We correlated fitted material constants with ECM composition measured by biochemical (ascending aorta) or histological (carotid artery) methods. We show significant correlations between ECM composition and material parameters for the mean values for each group, with biochemical measurements correlating more strongly than histological measurements. Understanding how arterial stiffening depends on age, sex, ECM composition, and artery type may help design effective, personalized clinical treatment strategies. [DOI: 10.1115/1.4063272]

Introduction

Large artery stiffening is both a cause and a consequence of cardiovascular disease and occurs during natural aging [1]. Males and females have different susceptibilities for cardiovascular diseases related to large artery stiffening, such as hypertension and aneurysms, and also have a different timeline for arterial stiffening during aging [2]. One cause of arterial stiffening is a shift in the amount or organization of the dominant extracellular matrix (ECM) proteins in the artery, collagen, and elastin [3]. Collagen fibers provide strength and limit distension at high pressures, whereas elastic fibers, composed primarily of elastin, provide elasticity and allow the arteries to expand during systole and recoil during diastole pushing blood to distal tissues. Elastic fibers undergo fragmentation with aging that results in a transfer of load to the stiffer collagen fibers, causing overall stiffening of the arterial wall [4]. Characterization of ECM degradation patterns and mechanical remodeling of large arteries in men and women with aging and disease may help us to better understand and treat arterial stiffening in a patient-specific manner.

Animal models can be used to investigate how changes in ECM proteins are related to arterial stiffening and cardiovascular disease and allow for well-controlled investigation of sex differences that can be challenging in the clinic. In particular, elastin heterozygous ($Eln^{+/-}$) mice have ~60% of wildtype ($Eln^{+/+}$) elastin levels, increased arterial stiffness, and hypertension [5]. However, they are able to maintain a physiologic elastic modulus near wildtype values in the ascending aorta, the largest elastic artery, throughout postnatal growth and adulthood due to geometric remodeling and ECM reorganization [6]. Additionally, male $Eln^{+/-}$ mice have an altered vascular aging process that suggests early arterial remodeling may help them adapt to later changes with aging [7]. We previously showed that elastin haploinsufficiency has divergent effects on arterial remodeling with aging that depends on sex [8]. However, at

[1]Corresponding author.

Manuscript received February 14, 2023; final manuscript received August 11, 2023; published online March 7, 2024. Assoc. Editor: Sara Roccabianca.

the time we only presented circumferential mechanical behavior and elastic arteries are subjected to biaxial loading in vivo.

Biaxial mechanical data from mouse arteries have previously been fitted with 2- or 4-fiber Holzapfel–Gasser–Ogden (HGO) [9]-type constitutive models for biomechanical phenotyping in aging and disease [10]. These studies provide insight into how biomechanical parameters such as physiologic stored strain energy, stresses, moduli, and strains adapt in an attempt to maintain homeostatic (i.e., young and wildtype) values and possible microstructurally based explanations for changes in mechanical behavior [11]. The HGO models have built-in coupling between fiber and cross-fiber deformations and a discrete number of fiber families. Dong and Sun [12] recently proposed a novel unified-fiber distribution (UFD) constitutive model [13] that does not require a specified number of fiber families and can have varied amounts of deformation coupling. In addition, the UFD model only has four material constants, reducing the likelihood of obtaining nonunique material constants as compared to HGO-type models with increased numbers of material constants. Here, we evaluated the ability of the UFD model to fit biaxial mechanical data of an elastic artery (ascending aorta) and a muscular-elastic artery (common carotid) in young and old, male and female, $Eln^{+/+}$ and $Eln^{+/-}$ mice and interpret material property and biomechanical phenotype changes as a function of age, sex, and ECM composition.

Methods

Animals. Male and female $Eln^{+/+}$ *and* $Eln^{+/-}$ [14] mice in a C57BL/6J background at 6 and 24 months of age were used in this study. All animal procedures were approved by the Institutional Animal Care and Use Committee of Washington University in St. Louis. Mice were sacrificed by CO_2 overdose. Stereo micrographs were taken for in situ length measurements [8] and the ascending aorta (ASC), left common carotid (LCC), and right common carotid (RCC) were all excised, cleaned, and stored in physiologic saline solution for up to 3 days at 4 °C before use [15].

Passive Biaxial Mechanical Testing. The LCC or ASC was mounted on custom, stainless steel cannulae in a pressure myograph (110P, Danish Myotechnology), submerged in physiologic saline solution at 37 °C, and secured by 6-0 sutures, as previously described [8]. Each artery was preconditioned by cyclic pressurization and axial stretch for three cycles. Each artery was then inflated from 0 to 175 mmHg in 25 mmHg pressure steps at a rate of 2 mmHg/s and a hold time of 30 s/step while being held at three different axial stretch values for three cycles, then axially stretched from the minimum to maximum axial stretch values while being held at 50, 100, and 150 mmHg for three cycles. Axial stretch values were chosen to bracket the in situ stretch and were approximately 1.4–2.0 for the LCC and 1.0–1.7 for the ASC. The pressure, outer diameter, and force were recorded at 1 Hz. The axial stretch at each time point was determined assuming a constant stretch rate while manually turning the axial micrometer. The third loading cycle was used for further data analysis. After testing, each artery was cut into rings and imaged for unloaded dimension measurements. The rings and remaining tissue from the ASC were stored at −80 °C for protein quantification. The unloaded dimensions and the pressure-diameter mechanical testing data near the in situ axial stretch were previously reported [8]. Here, we use additional mechanical testing protocols to better characterize the biaxial properties of these arteries.

Histology. Representative histology images of the RCC were previously shown [8], but were not quantified. Briefly, the RCC was fixed in 10% formalin, dehydrated in a graded series of ethanol, embedded in paraffin, and sectioned. Verhoeff Van Gieson (VVG) and picrosirius red (PSR) staining were performed and imaged to visualize elastic laminae and collagen fibers, respectively. The entire arterial area captured in 20× brightfield micrographs was analyzed using custom-MATLAB scripts to separate the media and adventitia and then quantify the amount of ECM constituents in the media using a pixel-wise detection based on the hue, saturation, and lightness (*HSL*) of color values [16]. For VVG images, the media was separated from the adventitia by identifying the black pixels of elastin and then converting the image to a binary mask. Using a series of morphological operations to close and fill the elastin mask, areas of the RCC that were inside (media) and outside (adventitia) of the external elastic lamina were identified and separated. After automatic separation, the media and adventitia regions were manually refined by the user, if necessary. For PSR images, the media was manually separated from the adventitia by user-defined tracing and refinement of the border between the media (light red/pink staining) and adventitia (dark red staining). For quantification of medial VVG images, elastin was first defined as $H = 0$ deg–360 deg, $S = 0$–1, $L = 0$–0.3 (black—very dark) and then remaining other tissue was defined as $H = 0$ deg–360 deg, $S = 0$–1, $L = 0.1$–0.99 (all colors except white). For quantification of medial PSR images, collagen was first defined as $H = 260$ deg –25 deg, $S = 0.1$–1, $L = 0.1$–0.6 (dark violet–red) and then other tissue was defined as $S = 340$ deg–75 deg, $S = 0.1$–1, $L = 0.2$–0.9 (pink–yellow). Despite some overlapping *HSL* parameters, pixels were assigned to only one constituent based on the order of color detection. The images were analyzed by users blinded to the age, sex, and genotype of the mouse. Correlations between RCC ECM composition and LCC material constants were examined.

Protein Quantification. Elastin, collagen, and total protein ratios were previously reported for the ASC [8]. Briefly, total protein was determined with a ninhydrin assay [17], elastin was determined by a competitive ELISA [18], and collagen was determined by measuring hydroxyproline (13.5% of collagen by mass) through a Chloramine T reaction [19]. Correlations between ASC ECM composition and material constants were examined.

Mechanical Testing Data Analysis. The arteries are assumed to be incompressible cylinders with no shear. The midwall stretch ratios (λ) in the axial (z) and circumferential (θ) directions are defined by

$$\lambda_z = \frac{l}{L} \tag{1a}$$

$$\lambda_\theta = \frac{r_i + r_o}{R_i + R_o} \tag{1b}$$

where l and L are the deformed and undeformed lengths, R and r are the undeformed and deformed radii, and the subscripts i and o correspond to the inner and outer surfaces, respectively. The average Cauchy stresses (σ) in the axial and circumferential direction are

$$\sigma_z = \frac{f + P\pi r_i^2}{\pi\left(r_o^2 - r_i^2\right)} \tag{2a}$$

$$\sigma_\theta = \frac{P r_i}{r_o - r_i}, \tag{2b}$$

where P is the measured pressure and f is the measured axial force.

Constitutive Modelling. Inflation and extension of the arteries can be described by the deformation gradient ($\boldsymbol{F}$) and the right Cauchy–Green ($\boldsymbol{C}$) strain tensors,

$$\boldsymbol{F} = \mathrm{diag}[\lambda_r, \lambda_\theta, \lambda_z] \tag{3a}$$

$$\boldsymbol{C} = \mathrm{diag}\left[\lambda_r^2, \lambda_\theta^2, \lambda_z^2\right] \tag{3b}$$

where r denotes the radial direction. Based on the HGO model [9], the passive strain energy ($\bar{\Psi}$) for a biologic tissue can be defined as the sum of a matrix (m) component and a fibrous (f)

component, $\bar{\Psi} = \bar{\Psi}_m + \bar{\Psi}_f$. The strain energy of the isotropic, Neo-Hookean matrix component is

$$\bar{\Psi}_m = \frac{1}{2} c(\bar{I}_1 - 3) \tag{4}$$

where c is a material constant, $\bar{I}_1 = tr(\bar{\boldsymbol{C}})$, $\bar{\boldsymbol{C}} = J^{-\frac{2}{3}}\boldsymbol{C}$, $\boldsymbol{C} = \boldsymbol{F}^T\boldsymbol{F}$, $J = det\,\boldsymbol{F}$. Based on the UFD model [12], the strain energy of the anisotropic, nonlinear fibrous component depends on the degree of deformation coupling (medium or strong) and the overall fiber orientation

$$\bar{\Psi}_{f-\text{Medium}} = \frac{k_1}{2k_2}\left\{\exp\left[k_2\left(\delta_{\|}\bar{E}_{\|}^2 + \delta_{\perp}\bar{E}_{\perp}^2\right)\right] - 1\right\} \tag{5a}$$

or

$$\bar{\Psi}_{f-\text{Strong}} = \frac{k_1}{2k_2}\left\{\exp\left[k_2\left(\delta_{\|}\bar{E}_{\|} + \delta_{\perp}\bar{E}_{\perp}\right)^2\right] - 1\right\} \tag{5b}$$

where k_1 and k_2 are material constants, $\delta_{\|} = H(\bar{I}_4 - 1)$, $\delta_{\perp} = H(\bar{I}_{4\perp} - 1)$, where $H =$ the Heaviside step function, which isolates the fibrous contribution to tension only, $\bar{I}_4 = (a_o \otimes a_o) : \bar{\boldsymbol{C}}$ and $\bar{I}_{4\perp} = (a_{0\perp} \otimes a_{0\perp}) : \bar{\boldsymbol{C}}$, where a_o and $a_{0\perp}$ are unit vectors representing the symmetric mean (assumed to be circumferential in this case) and perpendicular (assumed to be axial in this case) fiber directions, respectively. The strain terms $(\bar{E}_{\|}, \bar{E}_{\perp})$ are defined by

$$\bar{E}_{\|} = (1 - \zeta)\,(\bar{I}_4 - 1) \tag{6a}$$

$$\bar{E}_{\perp} = (\zeta)\,(\bar{I}_{4\perp} - 1) \tag{6b}$$

where ζ is a scalar material constant characterizing the average fiber component in the $a_{0\perp}$ direction in an integral sense and ranging within [0,1] for a general planar distribution of multiple fiber families.

$\bar{\Psi}_{f-\text{Strong}}$ is mathematically equivalent to the HGO model [20] and strongly couples stress in one planar direction to stretch in the perpendicular planar direction [12]. $\bar{\Psi}_{f-\text{Medium}}$ has less strong deformation coupling between stress and stretch in different planar directions. These two strain energy functions for the fibrous component allow investigation of how coupling between different directions may change with artery type, age, sex, and ECM composition.

The calculated Cauchy stress ($\boldsymbol{\sigma}_{\text{calc}}$) can be determined by

$$\boldsymbol{\sigma}_{\text{calc}} = 2\boldsymbol{F}\frac{\partial \bar{\Psi}}{\partial \bar{\boldsymbol{C}}}\boldsymbol{F}^T - p\boldsymbol{I} \tag{7}$$

where $p =$ hydrostatic pressure and $\boldsymbol{I} =$ the identity tensor. The calculated pressures and forces for the constitutive model stresses were determined from Eqs. (2*a*) and (2*b*). The material constants (c, k_1, k_2, ζ) were determined by minimizing the error between the experimentally measured ($p_{\text{exp}}, f_{\text{exp}}$) and calculated ($p_{\text{calc}}, f_{\text{calc}}$) pressures and axial forces

$$\text{error} = \frac{\sum (p_{\text{exp}} - p_{\text{calc}})^2}{\sum (p_{\text{exp}})^2} + \frac{\sum (f_{\text{exp}} - f_{\text{calc}})^2}{\sum (f_{\text{exp}})^2} \tag{8}$$

using the MATLAB function *fmincon*. The material constants were constrained to the positive domain and ζ was limited between 0 and 1. Multiple initial guesses were used to encourage identification of a global minimum. Only those arteries with six successful mechanical testing protocols (i.e., pressurization at three fixed axial stretches and axial stretch at three fixed pressures) were included in the constitutive modeling.

Individual fitted material constants were used along with average systolic blood pressures for each group (Table 1) and in situ/physiologic axial stretches for each artery from Hawes et al. [8] to determine physiologic biomechanical parameters such as circumferential stretch, circumferential and axial stresses, circumferential and axial incremental moduli, and stored strain energy. Incremental elastic moduli in the axial (ξ_z) and circumferential (ξ_θ) directions were calculated by [21]

Table 1 Average systolic blood pressure (mmHg) from Hawes et al. [8] for each group

	Males		Females	
	$Eln^{+/+}$	$Eln^{+/-}$	$Eln^{+/+}$	$Eln^{+/-}$
6 months	106	109	104	111
24 months	114	115	117	120

$$\xi_z = 4\lambda_z^2\frac{\partial \bar{\Psi}}{\partial C_{zz}} + 4\lambda_z^4\frac{\partial^2 \bar{\Psi}}{\partial C_{zz}^2} \tag{9a}$$

$$\xi_\theta = 4\lambda_\theta^2\frac{\partial \bar{\Psi}}{\partial C_{\theta\theta}} + 4\lambda_\theta^4\frac{\partial^2 \bar{\Psi}}{\partial C_{\theta\theta}^2} \tag{9b}$$

using the physiologic biaxial stretch values for each artery.

Statistical Comparisons. Three-way analysis of variance (ANOVA) was performed to determine the effects of age, sex, genotype, and their interactions. Correlation analyses were performed to examine relationships between ECM composition and material constants. Pearson r values and goodness of fit (R^2) are reported. All statistical analyses were performed with Prism (GraphPad). P-values less than 0.05 were considered significant.

Results

Best Fit Model and Material Constants. Passive biaxial mechanical data for the LCC, which is a muscular-elastic artery, have a better fit to $\bar{\Psi}_{f-\text{medium}}$ ($R^2 = 0.76 \pm 0.05$) than $\bar{\Psi}_{f-\text{strong}}$ ($R^2 = 0.64 \pm 0.08$) (example fits in Figs. 1(*a*)–1(*d*)). The ASC, which is the most elastic artery in the body, has a better fit to $\bar{\Psi}_{f-\text{Strong}}$ ($R^2 = 0.80 \pm 0.05$) than $\bar{\Psi}_{f-\text{medium}}$ ($R^2 = 0.47 \pm 0.21$) (example fits in Figs. 1(*e*) and 1(*f*)). These results are consistent with fitting of the HGO model [20], which is mathematically equivalent to $\bar{\Psi}_{f-\text{Strong}}$ [12] and has similar R^2 values to $\bar{\Psi}_{f-\text{Strong}}$ for both arteries (not shown). R^2 and fitted parameters for all arteries and both UFD coupling models are presented in Tables 1 and 2 available in the Supplemental Materials on the ASME Digital Collection. As there was a clear difference in the ability of each UFD coupling model to fit each artery type, all subsequent analyses were performed only with the best fit model. Mean R^2 of the best fit model for each group ranges from 0.74 to 0.84, with ASC having higher R^2 overall than LCC (Figs. 2(*a*) and 3(*a*)). The best fit UFD coupling model depends solely on artery type and not sex, age, or genotype, indicating that directional coupling may be inherent to the ECM organization associated with each artery type.

For LCC with medium deformation coupling, sex has a significant effect on all fitted material constants except ζ; age has a significant effect on k_2 and k_1/k_2; and genotype has a significant effect on c, k_2, and ζ (Fig. 2). The constant, c, associated with the isotropic matrix component (Eq. (4)) is lower in $Eln^{+/-}$ than $Eln^{+/+}$ LCC and lower in females compared to males (Fig. 2(*b*)). The constant k_1, a constant for the anisotropic, nonlinear fibrous component (Eq. (5*a*)), is higher in female LCC than male (Fig. 2(*c*)). The constant k_2, the exponential constant for the anisotropic, nonlinear fibrous component (Eq. (5*a*)), is lower in female LCC than male, higher in $Eln^{+/-}$ than $Eln^{+/+}$, and higher in 24 month-old compared to 6 month-old (Fig. 2(*d*)). The constant, ζ, which is a measure of the average fiber contribution in the perpendicular direction (axial) to the average fiber orientation (circumferential), is higher in $Eln^{+/-}$ LCC than $Eln^{+/+}$. Overall, the results indicate that male sex, 24 months of age, and $Eln^{+/-}$ genotype tend toward more nonlinear contributions and

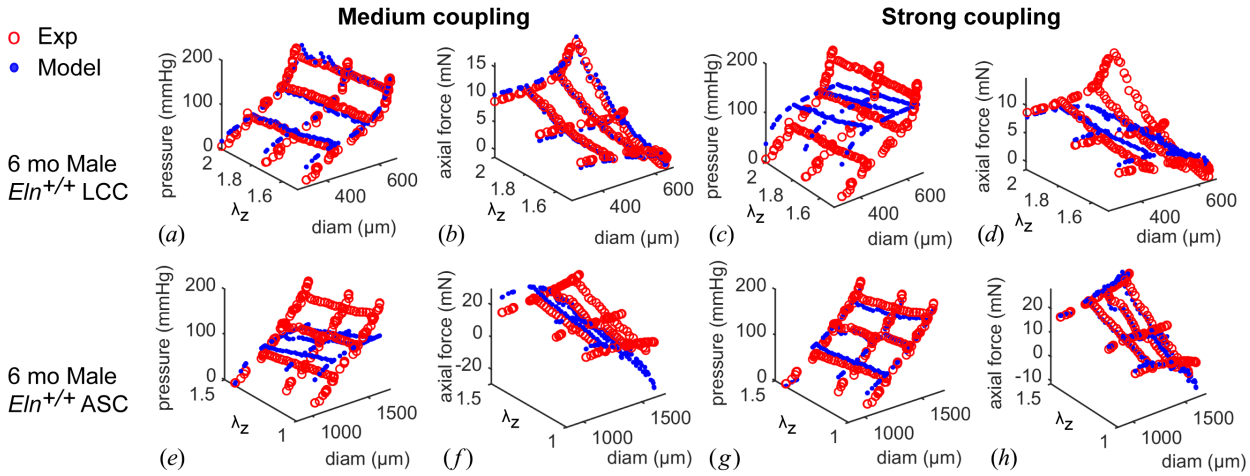

Fig. 1 Representative experimental data and constitutive model predictions for a 6-month-old male $Eln^{+/+}$ LCC ((*a*)–(*d*)) and ASC ((*e*) and (*f*)). Six experimental protocols are shown where each artery was held at three constant axial stretch values (λ_z) while pressure was increased and held at three constant pressure values while the axial stretch was increased. Pressure, axial force, outer diameter (diam), and axial stretch were recorded. The medium-coupled UFD model ((*a*) and (*b*)) fits better than the strongly coupled UFD model ((*c*) and (*d*)) to LCC data while the strongly coupled UFD model ((*g*) and (*h*)) fits better than the medium-coupled UFD model ((*e*) and (*f*)) to ASC data.

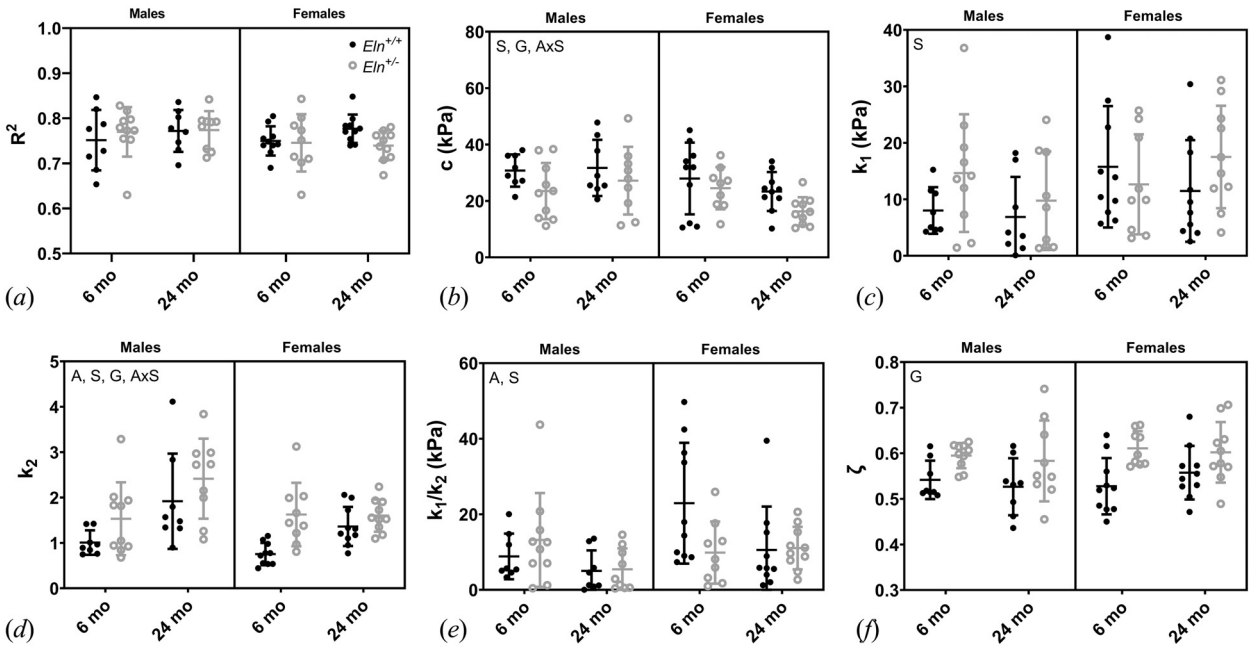

Fig. 2 Fitted constitutive model constants for LCC. The medium-coupled UFD model best fits LCC independent of age, genotype, and sex (R^2, *a*). Constant *c* (*b*) is associated with the isotropic, Neo-Hookean matrix component and constants k_1 (*c*) and k_2 (*d*) are associated with the anisotropic, nonlinear fibrous component. The ratio k_1/k_2 (*e*) is a measure of the overall linearity. ζ (*f*) is a scalar representing the contribution of the fibrous component in the direction (axial) perpendicular to the preferred direction (circumferential). Letters in the panels indicate significant differences for age (A), genotype (G), and/or sex (S) by three-way ANOVA. $N = 8$–10 per group.

also that $Eln^{+/-}$ genotype tends toward more axial contributions of the fibrous component for the LCC mechanical behavior captured in this study.

For ASC with strong deformation coupling, sex has a significant effect on R^2, c, and k_1; age has a significant effect on k_2, k_1/k_2, and ζ; and genotype has a significant effect on all fibrous material constants (Fig. 3). Male ASC has a higher R^2 (Fig. 3(*a*)), lower c (Fig. 3(*b*)), and higher k_1 (Fig. 3(*c*)) than female. 24-month-old ASC has a higher k_2 (Fig. 3(*d*)), lower k_1/k_2 (Fig. 3(*e*)) and lower ζ (Fig. 3(*f*)) than 6-month-old ASC. $Eln^{+/-}$ ASC has lower k_1 (Fig. 3(*c*)), higher k_2 (Fig. 3(*d*)), lower k_1/k_2 (Fig. 3(*e*)), and higher ζ (Fig. 3(*f*)) than $Eln^{+/+}$. Similar to LCC, 24 months of age and $Eln^{+/-}$ genotype tend to more nonlinear behavior for ASC, but unlike LCC, male sex does not tend to exhibit more nonlinear behavior for ASC. Similar to LCC, $Eln^{+/-}$ genotype tends toward more axial contributions for the fibrous component in ASC, but unlike LCC, 24 months of age reduces the axial component contribution in ASC. The quality of fit and material constant values show artery dependent deformation coupling and variation of the isotropic matrix and anisotropic fibrous material constants that depend on artery type, age, sex, and genotype.

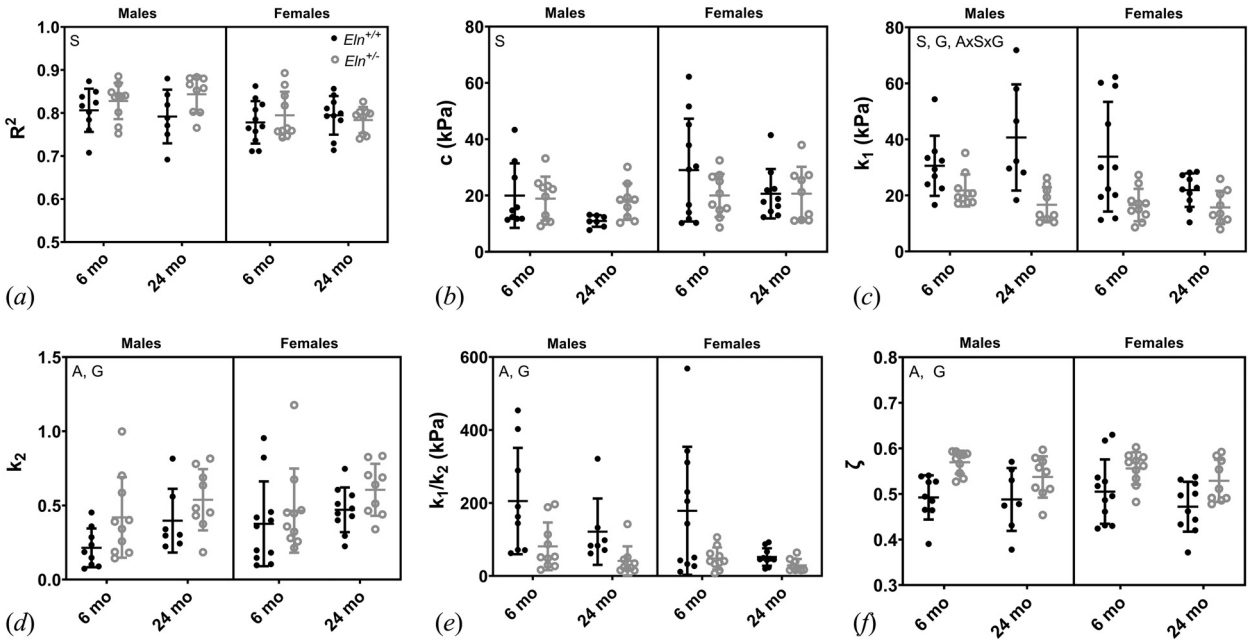

Fig. 3 Fitted constitutive model constants for ASC. The strongly coupled UFD model best fits ASC independent of age, genotype, and sex (R^2, *a*). Constant *c* (*b*) is associated with the isotropic, Neo-Hookean matrix component and constants k_1 (*c*) and k_2 (*d*) are associated with the anisotropic, nonlinear fibrous component. The ratio k_1/k_2 (*e*) is a measure of the overall linearity. ζ (*f*) is a scalar representing the contribution of the fibrous component in the direction (axial) perpendicular to the preferred direction (circumferential). Letters in the panels indicate significant differences for age (A), genotype (G), and/or sex (S) by three-way ANOVA. $N = 7–11$ per group.

Physiological Stretch, Stress, Modulus, and Strain Energy. Average systolic blood pressures (Table 1) for each age, sex, and genotype and in situ/physiologic axial stretches (Figs. 4(*d*) and 5(*d*)) for each artery from Hawes et al. [8] were used to determine physiologic biaxial loading conditions for calculation of biomechanical parameters from the fitted material constants. For LCC, axial stretch, circumferential and axial stress, circumferential and axial modulus, and strain energy are all significantly decreased in $Eln^{+/-}$ compared to $Eln^{+/+}$ (Fig. 4), indicating that LCC is not able to maintain a homeostatic biomechanical state in the face of reduced elastin levels. The homeostatic state is defined as the value for young (6-month-old), wildtype ($Eln^{+/+}$) arteries. Circumferential stress, axial stretch, axial stress, and strain energy are decreased in 24-month-old LCC compared to 6-month-old (Fig. 4), suggesting that LCC cannot maintain homeostatic stresses with aging and that 24-month–old LCC is not as effective as 6-month-old for storing (and returning) energy that reduces workload on the heart. Axial stretch is decreased in female LCC compared to male (Fig. 4(*d*)), which could point to different baseline levels of in situ/physiologic stretch that depend on sex.

For ASC, circumferential stretch and axial stretch, as well as axial stress, are the only biomechanical parameters significantly affected by genotype, indicating that ASC may be able to maintain a nearly homeostatic biomechanical state in the face of reduced elastin levels (Fig. 5). 24-month-old ASC has higher circumferential modulus (Fig. 5(*c*)) consistent with stiffening with aging, lower axial stretch (Fig. 5(*d*)) consistent with LCC, and lower strain energy (Fig. 5(*g*)) consistent with LCC and reduced energy storage capacity with aging. Similar to LCC, ASC axial stretch is affected by sex, and age and sex interact (Fig. 5(*d*)). In general, ASC shows less dependence of biomechanical parameters on age, sex, or genotype (Fig. 5) compared to LCC (Fig. 4), demonstrating the remarkable ability of ASC to adapt many of its biomechanical parameters to a range of conditions.

Stored Strain Energy Contours. The mean material constants for each group were used to generate stored strain energy contours [10] for LCC (Fig. 6) and ASC (Fig. 7). When the energy contour lines are closer together, this indicates stiffening, more nonlinear behavior of the artery. Additionally, the span of the energy contours in the *x*-direction is indicative of circumferential material stiffness, whereas the span in the *y*-direction indicates axial material stiffness. The shape of the contours in Fig. 6 shows that LCC is stiffer in the axial than circumferential direction, consistent with $\zeta > 0.5$ (Fig. 2(*f*)), and that there is material stiffening in both directions with aging, consistent with increased contributions of the nonlinear, fibrous component, especially its exponential constant (Fig. 2(*d*)). Interestingly, female, $Eln^{+/-}$ LCC starts out the stiffest at 6 months (Fig. 6(*d*)) and demonstrates negligible changes at 24 months (Fig. 6(*h*)), whereas as male $Eln^{+/-}$ LCC demonstrates biaxial stiffening at 24 months (Fig. 6(*f*)), relative to 6 months (Fig. 6(*b*)). Due to reductions in axial stretch (along the *y*-axis) in $Eln^{+/-}$ LCC, these arteries operate in a stored strain energy region (red dots) where the contours are less close together than their $Eln^{+/+}$ counterparts at 6 and 24 months. The shape of the contours in Fig. 7 shows that $Eln^{+/+}$ ASC is nearly isotropic in material stiffness ($\zeta \sim 0.5$, Fig. 3(*f*)), but $Eln^{+/-}$ ASC is stiffer in the axial direction ($\zeta > 0.5$, Fig. 3(*f*)). Compared to LCC, there are few apparent differences in ASC energy contours with aging, consistent with adaptability of ASC in maintaining a homeostatic biomechanical state. However, due to reductions in axial stretch (along the *y*-axis) with aging (Fig. 5(*d*)), the physiologic stored strain energy (red dots) in ASC decreases with age, especially in males.

Extracellular Matrix Composition and Correlations With Material Parameters. In RCC VVG images, elastin appears as black, wavy layers of elastic laminae between brown/pink/purple smooth muscle cells in the media, with bright pink collagen visible in the adventitia. Quantification of RCC VVG images shows no significant differences in medial elastin (black mask) or other tissue amounts (red mask) with age, sex, or genotype (Fig. 8). Although reductions in elastin protein amounts were previously found in $Eln^{+/-}$ common carotid artery compared to $Eln^{+/+}$ by biochemical methods [5], differences are not measurable by quantification of two-dimensional histological sections in this study. In RCC PSR images, collagen in the media appears as red

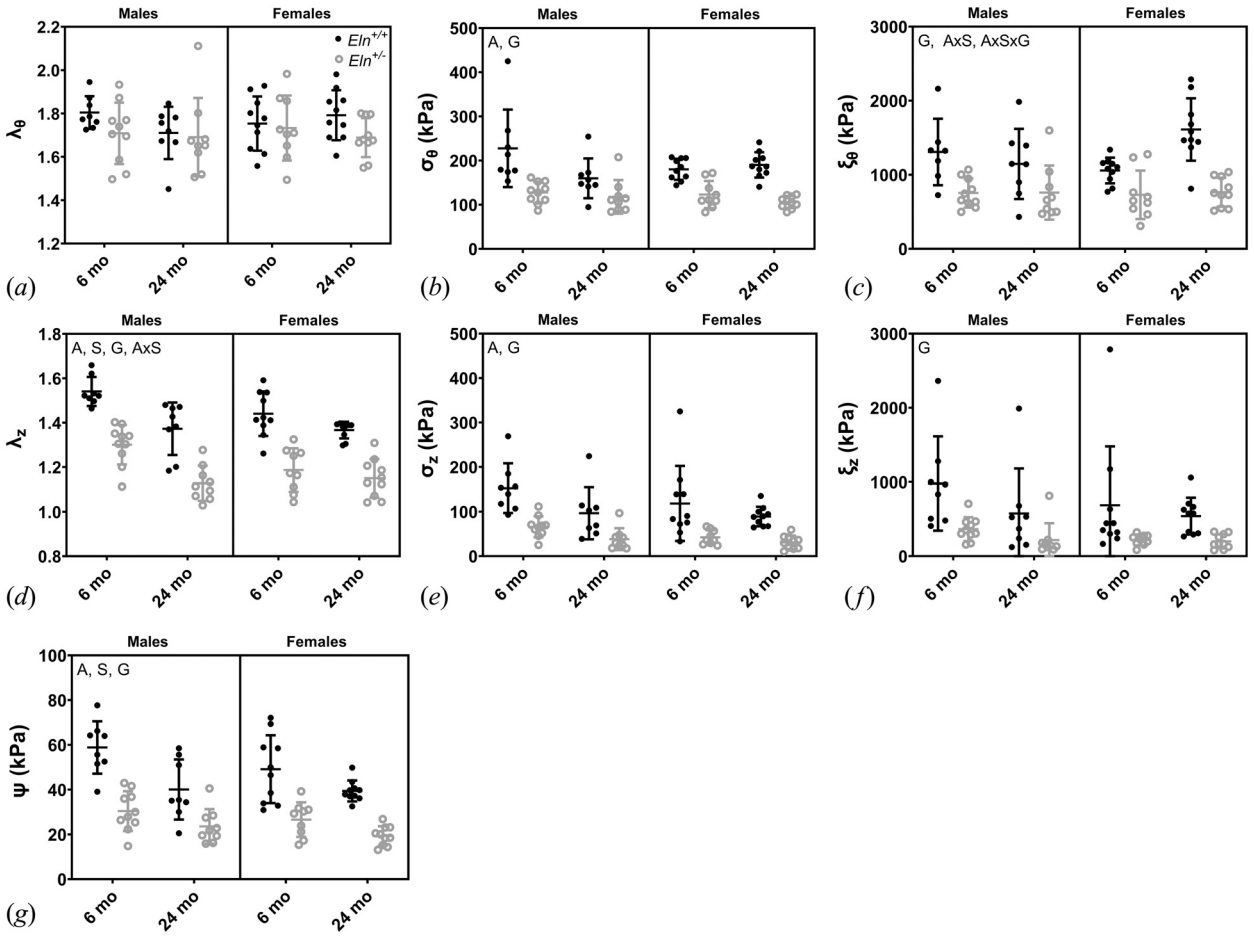

Fig. 4 Physiologic biomechanical parameters for LCC calculated from the fitted material constants for the medium coupled UFD model, the physiologic axial stretch, and the systolic pressure from each group [8]. Circumferential stretch (λ_θ, *a*), circumferential stress (σ_θ, *b*), circumferential modulus (ξ_θ, *c*), axial stretch (λ_z, *d*), axial stress (σ_z, *e*), axial modulus (ξ_z, *f*), and stored strain energy (Ψ) (*g*). Letters in the panels indicate significant differences for age (A), genotype (G), and/or sex (S) by three-way ANOVA. $N = 8$–10 per group.

staining outlining the yellow elastic laminae and intermixed with yellow/pink smooth muscle cells. Collagen in the adventitia is also red. Quantification of RCC PSR images shows increases in medial collagen amounts (red mask) and associated decreases in other tissue amounts (yellow mask) with $Eln^{+/-}$ genotype, 24 months of age, and male sex (Fig. 9). Interestingly, no differences were previously found in total collagen amounts between $Eln^{+/+}$ and $Eln^{+/-}$ common carotid arteries through biochemical methods [5], but differences are measurable through histological quantification of medial collagen amounts in this study.

Ascending aorta collagen and elastin amounts quantified through biochemical methods are shown in Hawes et al. [8] and reproduced in Fig. 10. ASC elastin and collagen amounts and elastin/collagen ratios for each group are consistent with previous biochemical results [5]. Elastin amounts and elastin/collagen ratios decrease with age, $Eln^{+/-}$ genotype, and female sex. Overall, the changes in elastin and collagen amounts determined through histological and biochemical methods support the idea that $Eln^{+/-}$ and aged arteries have decreased elastin/collagen ratios that may affect material constants and that there are sex-dependent differences in ECM composition.

Correlations between ECM composition and material constants for LCC/RCC and ASC were examined using mean values for each group to smooth out individual variations and avoid complications with not having the exact same tissue for multiple measurements (i.e., mechanical testing of the LCC and ECM composition from the RCC). For LCC/RCC, there are relatively strong correlations ($|r| \geq 0.45$) (Fig. 11(*a*)) for medial elastin/other tissue amounts and ζ (Fig. 11(*c*)) and for medial collagen/other tissue amounts and k_2 (Fig. 11(*d*)) or k_1/k_2. For ASC, there are even stronger correlations ($|r| > 0.7$) (Fig. 11(*b*)) for elastin or elastin/collagen amounts and k_1, k_2 (Fig. 11(*e*)) or k_1/k_2 (Fig. 11(*f*)) and for collagen amounts and k_2 or k_1/k_2. For both arteries, correlations between collagen amounts and k_2 are positive and k_1/k_2 are negative, demonstrating more nonlinear contributions of the anisotropic fibrous component with increasing collagen amounts. For both arteries, correlations between elastin or collagen amounts and material properties typically have opposite signs, indicating that changes in elastin and collagen amounts have opposing effects on mechanical behavior. For both arteries, correlations between ECM composition and the isotropic matrix parameter, c, are relatively weak suggesting that the contribution of this component is difficult to identify based on ECM quantification.

Discussion

Males and females have varying susceptibilities to cardiovascular diseases and divergent vascular aging processes, possibly due to differences in ECM remodeling [2]. Microstructurally based constitutive models can relate ECM changes to passive material property changes that may highlight remodeling mechanisms and sex differences. In this study, we quantified ECM composition and correlated the values with best fit biaxial material properties from a novel UFD model with varying degrees of directional coupling for two different elastic arteries in young and old, male and female, $Eln^{+/+}$ and $Eln^{+/-}$ mice.

Directional Coupling and Component Contributions. The UFD model includes three choices for directional coupling: strong, medium, and weak. Dong and Sun showed that medium coupling

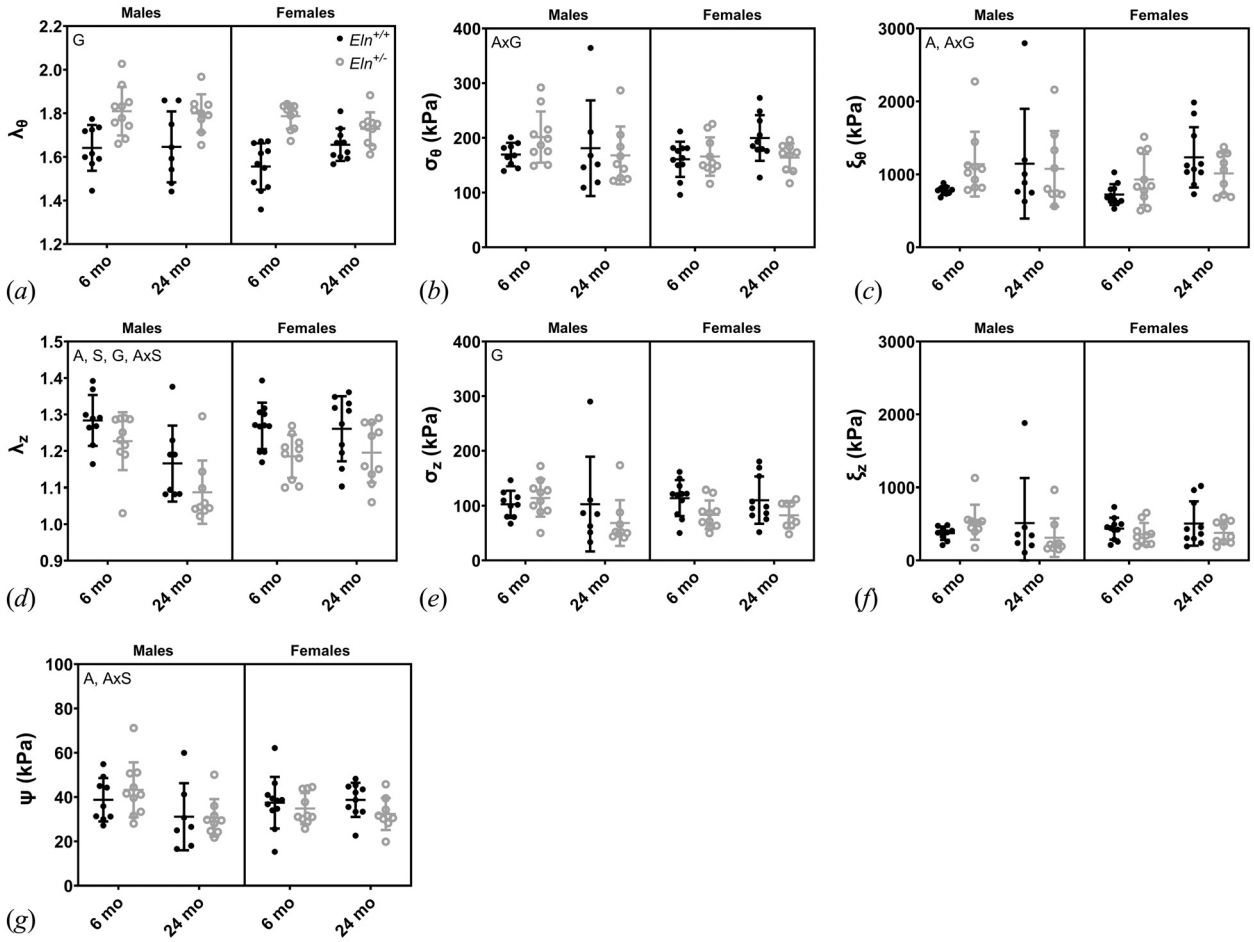

Fig. 5 Physiologic biomechanical parameters for ASC calculated from the fitted material constants for the strongly coupled UFD model, the physiologic axial stretch, and the systolic pressure from each group [8]. Circumferential stretch (λ_θ, *a*), circumferential stress (σ_θ, *b*), circumferential modulus (ξ_θ, *c*), axial stretch (λ_z, *d*), axial stress (σ_z, *e*), axial modulus (ξ_z, *f*), and stored strain energy (Ψ) (*g*). Letters in the panels indicate significant differences for age (A), genotype (G), and/or sex (S) by three-way ANOVA. $N = 7$–11 per group.

provides the best fit to planar biaxial data on the adventitia and the media of porcine aortic tissue [12]. In contrast, we find that strong coupling, which is mathematically equivalent to the HGO model [20], provides the best fit for cylindrical biaxial data for mouse ASC, but medium coupling provides the best fit for mouse LCC. Specifically, mouse ASC fit the strongly coupled UFD model and the HGO model (not shown) equally well, but mouse LCC did not fit the strongly coupled UFD model or the HGO model well and required the medium-coupled UFD model to reasonably approximate the mechanical behavior. Collectively, the results suggest that directional coupling of the fibrous component in vascular tissues may depend on the animal model, separation of the media and adventitial layers, and/or the artery type. The use of the UFD model allows for investigation into differences in directional coupling strength and eliminates the need to specify numbers of fiber families, which is difficult to identify precisely in biologic tissues. The UFD model with only four material constants reduces the likelihood for nonunique parameter fitting that can occur in nonlinear constitutive models with more constants, such as the four fiber HGO-type model with eight constants [22] while also allowing for directional coupling flexibility that significantly improves the goodness of fit for different artery types in our study.

Separation of stress contributions in the UFD model into an isotropic, Neo-Hookean material plus an anisotropic, nonlinear fibrous material allows evaluation as to how these different components may contribute to arterial mechanics as a function of age, sex, and elastin amounts. Our study provides results that are both consistent with and contradictory to expected contributions. For example, we previously showed using two- or three-fiber versions of the HGO model that the constant associated with the isotropic, Neo-Hookean material that is often attributed to elastin [9] is reduced in newborn mouse ASC from $Eln^{-/-}$ mice completely lacking elastin [23] (both sexes combined) and in 1–3 weeks old $Eln^{+/-}$ ASC [6] (males only). The Neo-Hookean material constant is the same in 1–2-months-old $Eln^{+/-}$ and $Eln^{+/+}$ male ASC [6], consistent with our current results for 6 and 24-month-old male and female $Eln^{+/-}$ and $Eln^{+/+}$ ASC. However, the Neo-Hookean material constant for 6 and 24-month-old $Eln^{+/-}$ male and female LCC is reduced compared to $Eln^{+/+}$, in line with the expected reduced contributions of this component due to reduced elastin amounts. In addition, the Neo-Hookean constant is significantly affected by sex, being generally lower in female LCC and higher in female ASC, compared to male. It is obvious that elastin amounts alone are not a sufficient explanation for changes in contribution of the Neo-Hookean material constant, but perhaps the results can give insight into the overall remodeling process that leads to altered arterial mechanics and stiffening that contributes to an increased risk of adverse cardiovascular events.

For the material constants associated with the anisotropic, nonlinear fibrous component, there is a consistent increase in k_2, the exponential constant, with aging and elastin haploinsufficiency in both arteries. While this increase in exponential behavior would be expected in a shift from elastin load bearing toward collagen load bearing [4], it also suggests remodeling of the fibrous component

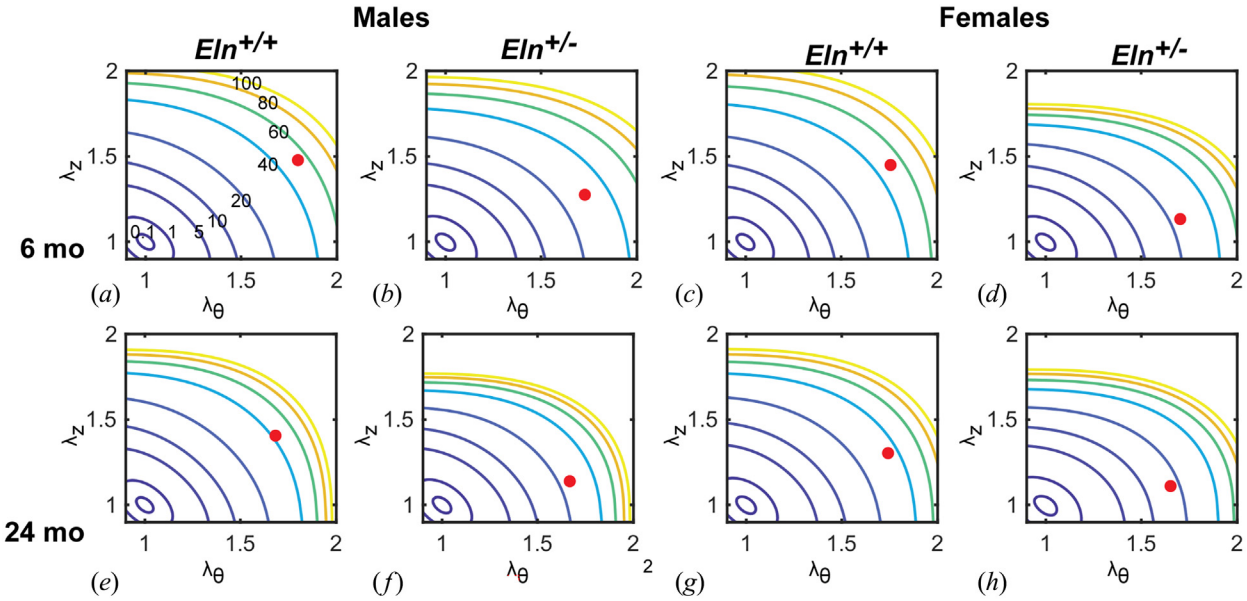

Fig. 6 Stored strain energy contours for LCC using the mean material constants of the medium coupled UFD model for each group over a range of circumferential (λ_θ) and axial (λ_z) stretch values: 6-month-old, male, $Eln^{+/+}$ (*a*); 6-month-old, male, $Eln^{+/-}$ (*b*); 6-month-old, female, $Eln^{+/+}$ (*c*); 6-month-old, female, $Eln^{+/-}$ (*d*); 24-month-old, male, $Eln^{+/+}$ (*e*); 24-month-old, male, $Eln^{+/-}$ (*f*); 24-month-old, female, $Eln^{+/+}$ (*g*); 24-month-old, female, $Eln^{+/-}$ (*h*). The colored lines indicate stored strain energy values in kPa as labeled in panel (*a*). The red dots indicate the physiologic biaxial stretch values.

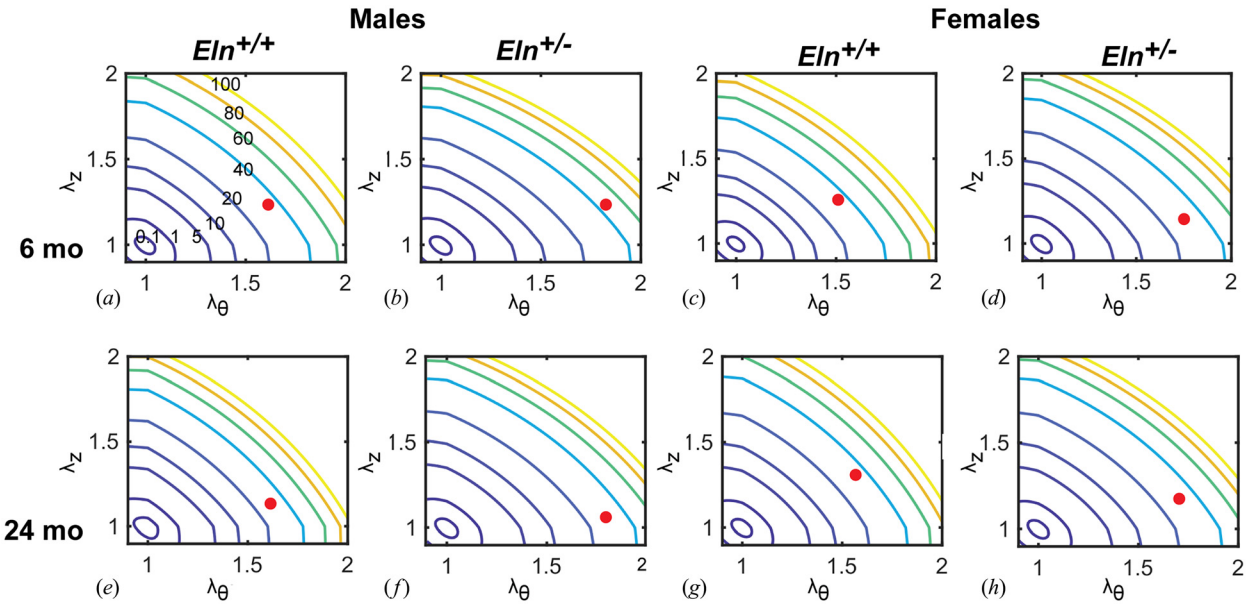

Fig. 7 Stored strain energy contours for ASC using the mean material constants of the strongly coupled UFD model for each group over a range of circumferential (λ_θ) and axial (λ_z) stretch values: 6-month-old, male, $Eln^{+/+}$ (*a*); 6-month-old, male, $Eln^{+/-}$ (*b*); 6-month-old, female, $Eln^{+/+}$ (*c*); 6-month-old, female, $Eln^{+/-}$ (*d*); 24-month-old, male, $Eln^{+/+}$ (*e*); 24-month-old, male, $Eln^{+/-}$ (*f*); 24-month-old, female, $Eln^{+/+}$ (*g*); 24-month-old, female, $Eln^{+/-}$ (*h*). The colored lines indicate stored strain energy values in kPa as labeled in panel (*a*). The red dots indicate the physiologic biaxial stretch values.

itself that contributes to more nonlinear behavior. This may be attributed to collagen fibers replacing smooth muscle cells [24], increases in medial [25] or adventitial [26] collagen amounts, or collagen crosslinking by nonenzymatic glycation [27], which are all evident with vascular aging. Increased nonlinearity could also be caused by decreased collagen fiber crimp, which has been seen in mouse arteries with genetically disrupted elastic fibers [28] or porcine aorta with enzymatically degraded elastic fibers [29]. We found increased collagen amounts by histological and biochemical methods, but did not investigate other factors such crosslinking or fiber crimp. There are sex differences in the material constants for the anisotropic fibrous component that may be due to sex hormones or arterial growth and aging rates that differ between males and females and could be investigated in future work to better understand arterial stiffening in individual patients.

Biomechanical Parameters and Remodeling. Arteries are under in situ axial stretch in the body. Our results of a decreased in situ axial stretch with aging and $Eln^{+/-}$ genotype are consistent

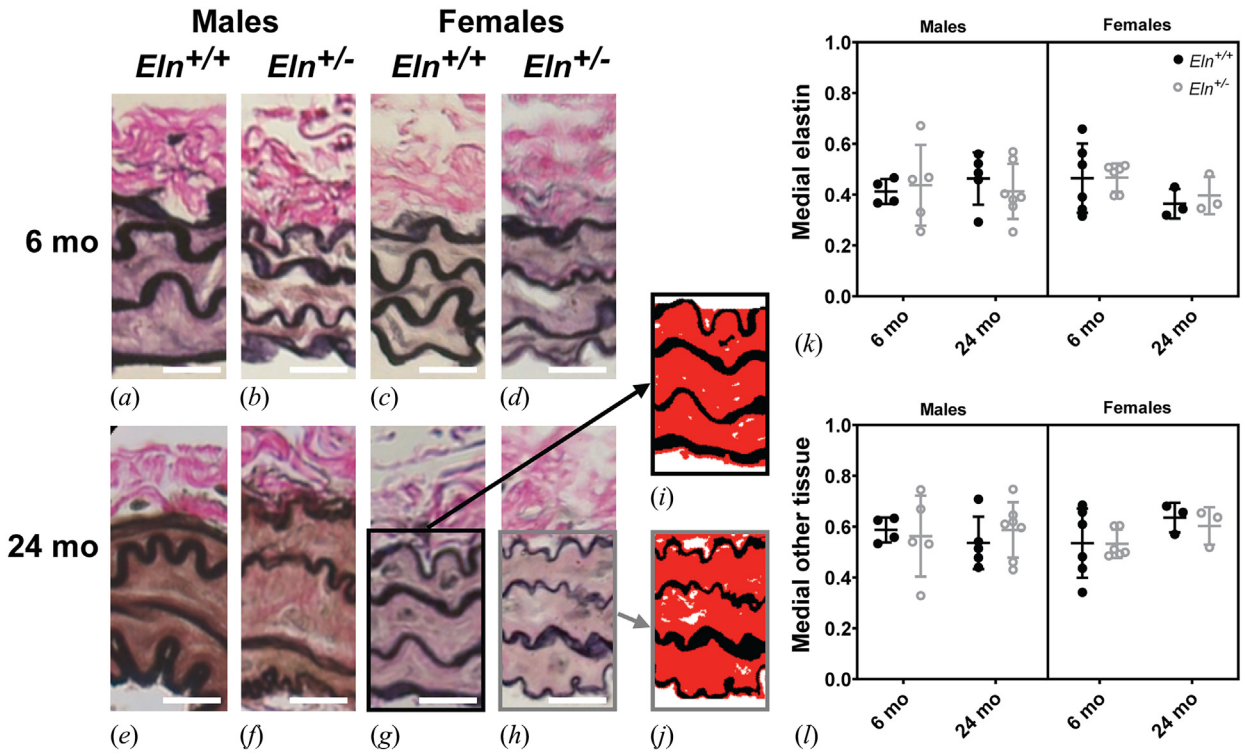

Fig. 8 VVG staining (*a*)–(*h*) of RCC shows elastin (black) and smooth muscle cells (brown/purple/pink) in the media and collagen (bright pink) in the adventitia. The lumen is at the bottom and scale bars = 20 μm. The medial VVG images were processed so that elastin is shown in black and other tissue is shown in red (*i*) and (*j*). Elastin (*k*) and other tissue (*l*) were quantified as a fraction of total medial area for each cross section. $N = 5–7$/group.

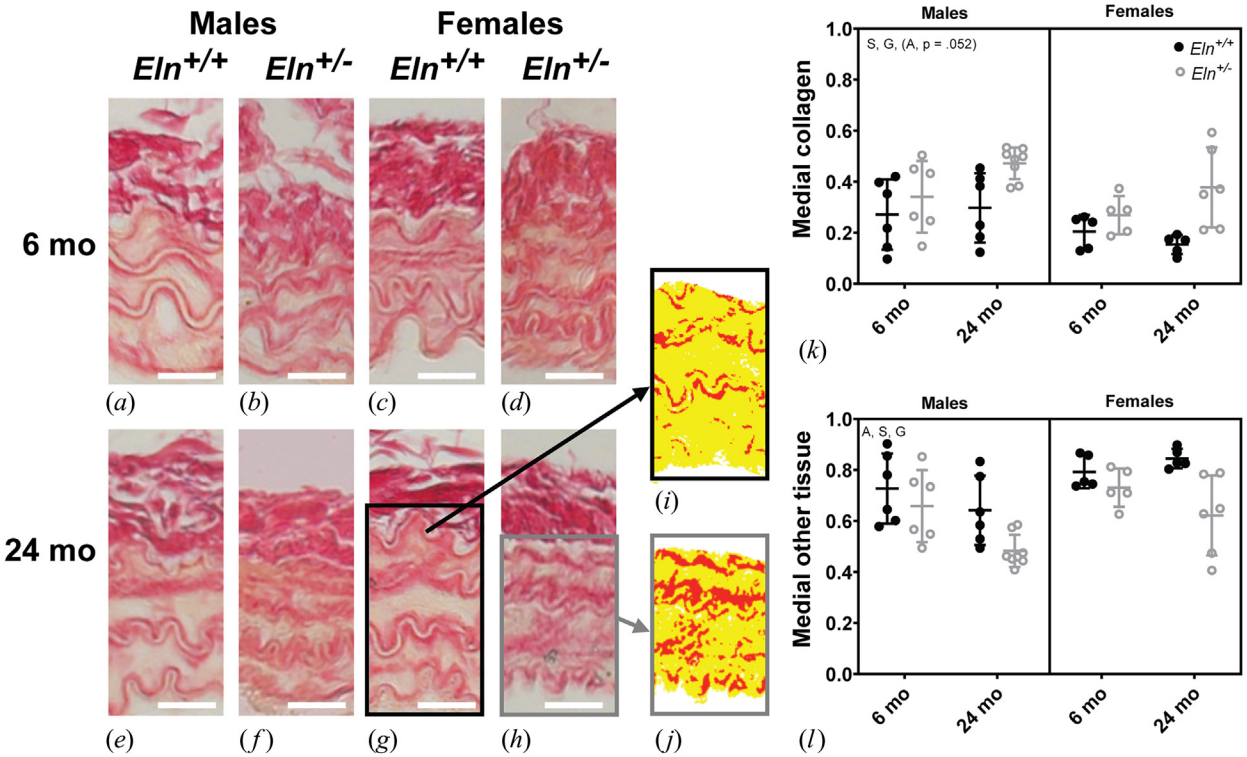

Fig. 9 PSR staining (*a*)–(*h*) of RCC shows collagen (red) in the adventitia and also outlining the elastic laminae (yellow) and interspersed with smooth muscle (yellow/pink) in the media. The lumen is at the bottom and scale bars = 20 μm. The medial PSR images were processed so that collagen staining is shown in red and other tissue is shown in yellow (*i*) and (*j*). Collagen (*k*) and other tissue (*l*) were quantified as a fraction of total medial area for each cross section. Letters in the panels indicate significant differences for age (A), genotype (G), and/or sex (S) by three-way ANOVA. $N = 5–7$/group.

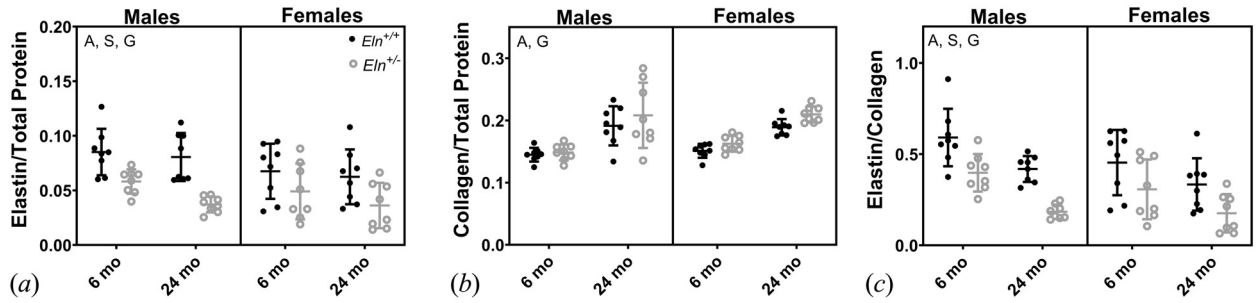

Fig. 10 Biochemical quantification of elastin (*a*), collagen (*b*), and elastin/collagen ratio (*c*) in ASC. Letters in the panels indicate significant differences for age (A), genotype (G), and/or sex (S) by three-way ANOVA. *N* = 8/group. Data reproduced from Hawes et al. [8].

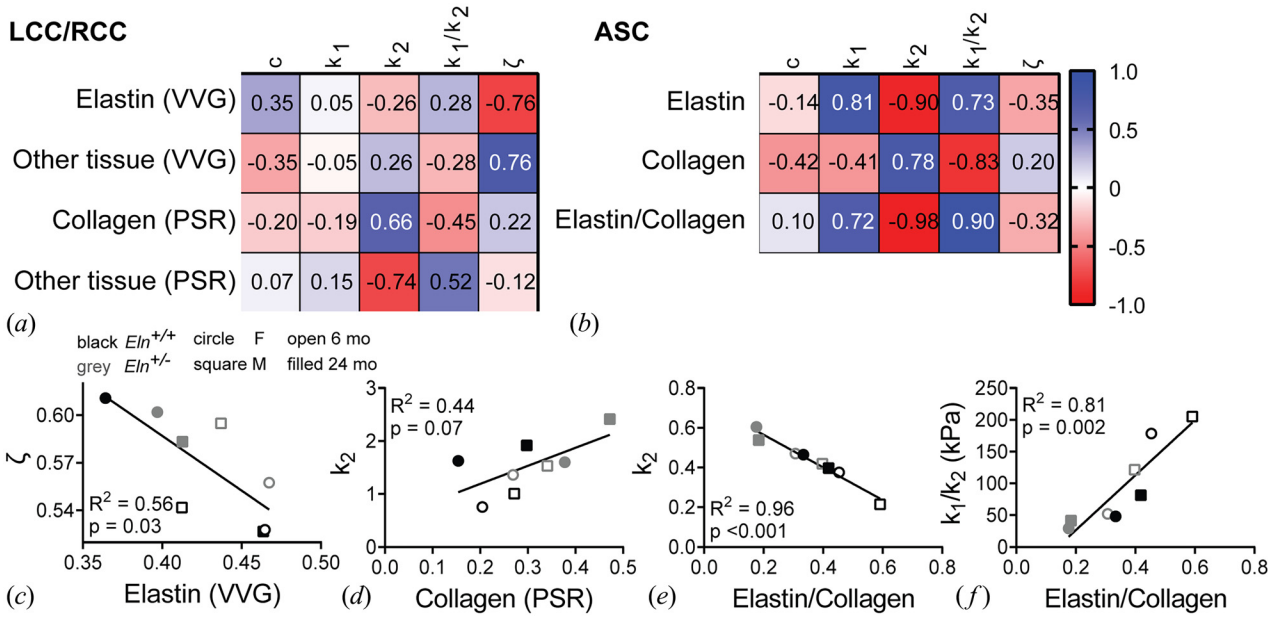

Fig. 11 Pearson r correlations between mean values for each group for fitted material constants from the medium coupled UFD model for LCC and histological ECM quantification for RCC (*a*) and between fitted material constants for the strongly coupled UFD model and biochemical ECM quantification for ASC (*b*). Specific linear correlations and *p*-values are shown for some pairs of interest for LCC/RCC (*c*) and (*d*) and ASC (*e*) and (*f*).

with previous results in mice demonstrating decreased axial stretch with elastic fiber fragmentation [28], elastin haploinsufficiency [30], aging [31], and also with more significant decreases in axial stretch with aging in LCC compared to ASC [32]. This decrease in axial stretch may be a compensatory adaptation to return stresses to homeostatic values, in response to perturbations in ECM composition or hemodynamics [33]. For LCC, the decrease in axial stretch appears to overcompensate because in many instances, the circumferential and axial stresses and moduli are reduced with elastin haploinsufficiency and aging. Arteries can grow and respond to increased [34] and decreased [35] axial stretch, and there is a complicated interplay between axial stretch and remodeling due to increased blood pressure [36], hence determining the biaxial loading state is critical for studies of mechanical remodeling.

The decreases in stress and moduli are counterintuitive to the observed increases in nonlinearity of the anisotropic fibrous component and increases in collagen amounts with aging and elastin haploinsufficiency. These findings imply that changes in the fibrous component nonlinearity do not play a significant role under physiologic loading conditions, but may become important with increased axial stretch or blood pressure. The average systolic pressures for each group were used to determine the physiologic biomechanical parameters and are increased with elastin haploinsufficiency and aging [8]. Hence, the stresses and moduli would be even lower in $Eln^{+/-}$ and 24-month-old arteries if there was not an increase in blood pressure. The circumferential and axial stresses and moduli are less affected by aging and elastin haploinsufficiency in the ASC compared to the LCC, suggesting that different arteries have varying remodeling capabilities. In both arteries, sex-specific differences are suggested in the axial compensatory response and outcomes. Ferruzzi et al. [32] found a decrease in circumferential and axial stress with aging in male ASC and LCC, but did not include female mice. Our divergent mechanical behavior between male and female arteries indicates a different pathology of remodeling with aging and ECM changes that warrants future investigation.

While the axial stretch adaptation is effective in modulating stresses, it decreases the overall stored strain energy of LCC and ASC with aging, compromising their ability to do work on the blood and perform the "Windkessel" function of elastic arteries to dampen pulsatile flows [37]. The stored strain energy depends on sex in LCC and has an interaction between age and sex in ASC, indicating that changes to the Windkessel function may follow a different timeline for males and females and may be important for understanding the risk of associated cardiovascular complications. The stored strain energy is reduced in LCC with elastin haploinsufficiency, but not in

ASC. Since the ASC receives the entire cardiac output, conserving its energy storage behavior may be critically important for cardiac function. Because stored strain energy depends on the applied stretches, as well as the material constants, the increased circumferential stretch in $Eln^{+/-}$ ASC may contribute to the homeostatic strain energy values. The increased ASC circumferential stretch also serves to expand the outlet diameter from the heart and maintain cardiac output, since $Eln^{+/-}$ arteries are overall smaller in diameter than their $Eln^{+/+}$ counterparts [5].

Correlations Between Elastin and Collagen Amounts and Material Constants. We looked at correlations between ECM composition (by histology or biochemistry) and material constants for the mean values for each group to determine if there were any structure–function relationships that could be deduced. Although the primary change in $Eln^{+/-}$ arteries is reduced elastin gene expression [14], this manifests as reduced elastin protein amounts measured biochemically [5,6]. Total collagen amounts are not increased in $Eln^{+/-}$ arteries to compensate for reduced elastin amounts [5,6,8]; hence, the ratio of elastin/collagen is reduced and would be expected to alter arterial mechanical behavior. In fact, we found significant correlations between several of the anisotropic fibrous material constants and elastin, collagen, and elastin/collagen ratios measured biochemically in ASC. As both ECM composition and some of the fibrous material constants (i.e., k_1) are sex dependent, this suggests a sex specific structure–function relationship that must be considered when evaluating changes in ASC mechanical behavior with age and/or elastin amounts.

Reduced elastin protein amounts in $Eln^{+/-}$ arteries are not apparent by histological staining, such as VVG, because $Eln^{+/-}$ arteries have slightly thinner, but more elastic laminae [8,14]. Thinning and disruption of elastic laminae with age and elastin haploinsufficiency in the mouse aorta are visible by electron microscopy, but not by light microscopy [7]. Increased collagen amounts measured biochemically with aging in ASC [8] are challenging to quantify histologically in mouse arteries because the adventitia (where the majority of collagen is located) is thin, not well-defined, and difficult to preserve during the fixation process. However, in examining PSR staining for collagen, we noted that collagen staining in the media appeared more diffusely distributed in $Eln^{+/-}$ and/or 24-month-old RCC compared to the distinctive collagen staining outlining elastic laminae in $Eln^{+/+}$ and/or 6-month-old RCC. This observation was confirmed by quantification of medial collagen amounts in RCC that increase with aging, $Eln^{+/-}$ genotype, and male sex. Ferruzzi et al. [32] and Pezet et al. [7] also found more collagen staining in the arterial media with aging and $Eln^{+/-}$ genotype, respectively, but only looked at male mice. Additionally, we found that collagen amounts correlate with several of the anisotropic fibrous material constants. Like ASC structure/function correlations, the results suggest a relationship between ECM composition and mechanical behavior that is sex dependent.

Previous work on biomechanical remodeling in mouse arteries includes studies with aging [32], aneurysmal disease [11], and hypertension/inflammation [38]. In general, these studies have focused on biomechanical parameters and how they are maintained at homeostatic values or not [32], how they correlate with disease indices such as arterial dilation [11], or how they correlate with inflammatory markers [38], providing a biomechanical phenotype that can be used to understand disease severity. These studies have used the 4-fiber HGO-type model that has eight unique material parameters, which well describes the arterial mechanical behavior, but does not typically provide a set of material constants that can be individually compared. The UFD model with four material constants and varied directional coupling provided good fits to mouse ASC and LCC in our study while providing material constants that can be attributed to different wall components and correlate with ECM composition. Material constants specific to age, sex, vessel type, and ECM composition are needed for a better understanding of biomechanical remodeling mechanisms and could be used to predict behavior under different loading conditions (such as hypertension), more complicated geometry (such as the curved ascending aorta), in fluid–solid-interaction models (to calculate fluid and solid stresses), and in growth and remodeling models (to predict mechanical evolution over time).

Limitations. Mechanical characterization is limited to our applied mechanical testing protocols, which encompass the physiologic range. We focused on passive mechanical properties and not on active mechanical properties, which are important for controlling blood flow in vivo. We also focused on ECM differences but have not included changes in cell numbers or cell phenotype that may contribute to variations in material constants. We quantified elastin and collagen amounts, but elastin and collagen density, crosslinking, orientation, microstructure, and integrity are also important for arterial mechanical behavior. We do not have a comparison of our ex vivo biomechanical data to in vivo arterial mechanical behavior; hence, our physiologic biomechanical parameters are an approximation that neglects factors such as arterial tone, connective tissue support, and variations in cardiovascular rhythm. Many differences between mice and humans exist in arterial wall structure, cardiovascular physiology, aging timeline, and disease susceptibility. However, the use of mice provides a model for detailed mechanical structure–function studies over a wide range of ages in different sexes that cannot readily be performed in humans.

Conclusions and Future Directions. We found that directional coupling for the best fit UFD constitutive model was different for LCC (muscular-elastic artery) and ASC (elastic artery). We identified best fit material constants that can help us understand how the arterial wall remodels with age, sex, and ECM composition. We found that ASC was able to better maintain a homeostatic biomechanical state than LCC, which may have implications for diseases that affect different vascular tree locations. We found significant correlations between some measures of ECM composition and anisotropic fibrous material constants, suggesting that the UFD models have the capacity to describe structure–mechanical function relationships for mouse arteries. We also found that several of the material constants and ECM composition values were sex dependent, indicating that males and females should be considered separately in evaluating arterial structure and its relationship to mechanical function. Arterial structure–function relationships could someday be used for patient-specific modeling and treatment regimens. Our work motivates future studies on sex differences in arterial mechanics and cardiovascular diseases associated with aging and ECM remodeling.

Funding Data

- National Institutes of Health (Grant Nos. R01 HL105314 and R56 HL152420; Funder ID: 10.13039/100000050).

References

[1] Mitchell, G. F., Hwang, S. J., Vasan, R. S., Larson, M. G., Pencina, M. J., Hamburg, N. M., Vita, J. A., Levy, D., and Benjamin, E. J., 2010, "Arterial Stiffness and Cardiovascular Events: The Framingham Heart Study," Circulation, **121**(4), pp. 505–511.

[2] Ogola, B. O., Zimmerman, M. A., Clark, G. L., Abshire, C. M., Gentry, K. M., Miller, K. S., and Lindsey, S. H., 2018, "New Insights Into Arterial Stiffening: Does Sex Matter?," Am. J. Physiol.: Heart Circ. Physiol., **315**(5), pp. H1073–H1087.

[3] Wagenseil, J. E., and Mecham, R. P., 2012, "Elastin in Large Artery Stiffness and Hypertension," J. Cardiovasc. Transl. Res., **5**(3), pp. 264–273.

[4] Greenwald, S. E., 2007, "Ageing of the Conduit Arteries," J. Pathology, **211**(2), pp. 157–172.

[5] Faury, G., Pezet, M., Knutsen, R. H., Boyle, W. A., Heximer, S. P., McLean, S. E., Minkes, R. K., Blumer, K. J., Kovacs, A., Kelly, D. P., Li, D. Y., Starcher, B., and Mecham, R. P., 2003, "Developmental Adaptation of the Mouse Cardiovascular System to Elastin Haploinsufficiency," J. Clin. Invest., **112**(9), pp. 1419–1428.

[6] Cheng, J. K., Stoilov, I., Mecham, R. P., and Wagenseil, J. E., 2013, "A Fiber-Based Constitutive Model Predicts Changes in Amount and Organization of

Matrix Proteins With Development and Disease in the Mouse Aorta," Biomech. Model. Mechanobiol., **12**(3), pp. 497–510.
[7] Pezet, M., Jacob, M. P., Escoubet, B., Gheduzzi, D., Tillet, E., Perret, P., Huber, P., Quaglino, D., Vranckx, R., Li, D. Y., Starcher, B., Boyle, W. A., Mecham, R. P., and Faury, G., 2008, "Elastin Haploinsufficiency Induces Alternative Aging Processes in the Aorta," Rejuvenation Res., **11**(1), pp. 97–112.
[8] Hawes, J. Z., Cocciolone, A., Cui, A. H., Griffin, D. B., Staiculescu, M. C., Mecham, R. P., and Wagenseil, J. E., 2020, "Elastin Haploinsufficiency in Mice Has Divergent Effects on Arterial Remodeling With Aging Depending on Sex," Am. J. Physiol.: Heart Circ. Physiol., **319**(6), pp. H1398–H1408.
[9] Holzapfel, G. A., Gasser, T. C., and Ogden, R. W., 2000, "A New Constitutive Framework for Arterial Wall Mechanics and a Comparative Study of Material Models," J. Elasticity, **61**(1/3), pp. 1–48.
[10] Ferruzzi, J., Bersi, M. R., and Humphrey, J. D., 2013, "Biomechanical Phenotyping of Central Arteries in Health and Disease: Advantages of and Methods for Murine Models," Ann. Biomed. Eng., **41**(7), pp. 1311–1330.
[11] Bellini, C., Bersi, M. R., Caulk, A. W., Ferruzzi, J., Milewicz, D. M., Ramirez, F., Rifkin, D. B., Tellides, G., Yanagisawa, H., and Humphrey, J. D., 2017, "Comparison of 10 Murine Models Reveals a Distinct Biomechanical Phenotype in Thoracic Aortic Aneurysms," J. R. Soc. Interface, **14**(130), p. 20161036.
[12] Dong, H., and Sun, W., 2021, "A Novel Hyperelastic Model for Biological Tissues With Planar Distributed Fibers and a Second Kind of Poisson Effect," J. Mech. Phys. Solids, **151**, p. 104377.
[13] Dong, H., Liu, M., Woodall, J., Leshnower, B. G., and Gleason, R. L., Jr., 2023, "Effect of Nonlinear Hyperelastic Property of Arterial Tissues on the Pulse Wave Velocity Based on the Unified-Fiber-Distribution (UFD) Model," Ann. Biomed. Eng., epub.
[14] Li, D. Y., Faury, G., Taylor, D. G., Davis, E. C., Boyle, W. A., Mecham, R. P., Stenzel, P., Boak, B., and Keating, M. T., 1998, "Novel Arterial Pathology in Mice and Humans Hemizygous for Elastin," J. Clin. Invest., **102**(10), pp. 1783–1787.
[15] Amin, M., Kunkel, A. G., Le, V. P., and Wagenseil, J. E., 2011, "Effect of Storage Duration on the Mechanical Behavior of Mouse Carotid Artery," ASME J. Biomech. Eng., **133**(7), p. 071007.
[16] Bersi, M. R., Collins, M. J., Wilson, E., and Humphrey, J. D., 2012, "Disparate Changes in the Mechanical Properties of Murine Carotid Arteries and Aorta in Response to Chronic Infusion of Angiotensin-II," Int. J. Adv. Eng. Sci. Appl. Math., **4**(4), pp. 228–240.
[17] Starcher, B., 2001, "A Ninhydrin-Based Assay to Quantitate the Total Protein Content of Tissue Samples," Anal. Biochem., **292**(1), pp. 125–129.
[18] Stoilov, I., Starcher, B. C., Mecham, R. P., and Broekelmann, T. J., 2018, "Measurement of Elastin, Collagen, and Total Protein Levels in Tissues," Methods Cell Biol., **143**, pp. 133–146.
[19] Jamall, I. S., Finelli, V. N., and Que Hee, S. S., 1981, "A Simple Method to Determine Nanogram Levels of 4-Hydroxyproline in Biological Tissues," Anal. Biochem., **112**(1), pp. 70–75.
[20] Gasser, T. C., Ogden, R. W., and Holzapfel, G. A., 2006, "Hyperelastic Modelling of Arterial Layers With Distributed Collagen Fibre Orientations," J. R. Soc. Interface, **3**(6), pp. 15–35.
[21] Baek, S., Gleason, R. L., Rajagopal, K. R., and Humphrey, J. D., 2007, "Theory of Small on Large: Potential Utility in Computations of Fluid-Solid Interactions in Arteries," Comput. Methods Appl. Mech. Eng., **196**(31–32), pp. 3070–3078.
[22] Bersi, M. R., Ferruzzi, J., Eberth, J. F., Gleason, R. L., Jr., and Humphrey, J. D., 2014, "Consistent Biomechanical Phenotyping of Common Carotid Arteries From Seven Genetic, Pharmacological, and Surgical Mouse Models," Ann. Biomed. Eng., **42**(6), pp. 1207–1223.
[23] Kim, J., Cocciolone, A. J., Staiculescu, M. C., Mecham, R. P., and Wagenseil, J. E., 2022, "Passive Biaxial Mechanical Behavior of Newborn Mouse Aorta With and Without Elastin," J. Mech. Behav. Biomed. Mater., **126**, p. 105021.
[24] Schlatmann, T. J., and Becker, A. E., 1977, "Histologic Changes in the Normal Aging Aorta: Implications for Dissecting Aortic Aneurysm," Am. J. Cardiol., **39**(1), pp. 13–20.
[25] Greenberg, S. R., 1986, "The Association of Medial Collagenous Tissue With Atheroma Formation in the Aging Human Aorta as Revealed by a Special Technique," Histol. Histopathol., **1**(4), pp. 323–326.
[26] Fleenor, B. S., Marshall, K. D., Durrant, J. R., Lesniewski, L. A., and Seals, D. R., 2010, "Arterial Stiffening With Ageing is Associated With Transforming Growth Factor-beta1-Related Changes in Adventitial Collagen: Reversal by Aerobic Exercise," J. Physiol., **588**(20), pp. 3971–3982.
[27] Schleicher, E. D., Wagner, E., and Nerlich, A. G., 1997, "Increased Accumulation of the Glycoxidation Product N(Epsilon)-(Carboxymethyl)Lysine in Human Tissues in Diabetes and Aging," J. Clin. Invest., **99**(3), pp. 457–468.
[28] Wan, W., Yanagisawa, H., and Gleason, R. L., Jr., 2010, "Biomechanical and Microstructural Properties of Common Carotid Arteries From Fibulin-5 Null Mice," Ann. Biomed. Eng., **38**(12), pp. 3605–3617.
[29] Chow, M. J., Turcotte, R., Lin, C. P., and Zhang, Y., 2014, "Arterial Extracellular Matrix: A Mechanobiological Study of the Contributions and Interactions of Elastin and Collagen," Biophys. J., **106**(12), pp. 2684–2692.
[30] Wagenseil, J. E., Nerurkar, N. L., Knutsen, R. H., Okamoto, R. J., Li, D. Y., and Mecham, R. P., 2005, "Effects of Elastin Haploinsufficiency on the Mechanical Behavior of Mouse Arteries," Am. J. Physiol.: Heart Circ. Physiol., **289**(3), pp. H1209–H1217.
[31] Brankovic, S., Hawthorne, E. A., Yu, X., Zhang, Y., and Assoian, R. K., 2019, "MMP12 Preferentially Attenuates Axial Stiffening of Aging Arteries," ASME J. Biomech. Eng., **141**(8), p. 081004.
[32] Ferruzzi, J., Madziva, D., Caulk, A. W., Tellides, G., and Humphrey, J. D., 2018, "Compromised Mechanical Homeostasis in Arterial Aging and Associated Cardiovascular Consequences," Biomech. Model. Mechanobiol., **17**(5), pp. 1281–1295.
[33] Humphrey, J. D., Eberth, J. F., Dye, W. W., and Gleason, R. L., 2009, "Fundamental Role of Axial Stress in Compensatory Adaptations by Arteries," J. Biomech., **42**(1), pp. 1–8.
[34] Jackson, Z. S., Gotlieb, A. I., and Langille, B. L., 2002, "Wall Tissue Remodeling Regulates Longitudinal Tension in Arteries," Circ. Res., **90**(8), pp. 918–925.
[35] Jackson, Z. S., Dajnowiec, D., Gotlieb, A. I., and Langille, B. L., 2005, "Partial Off-Loading of Longitudinal Tension Induces Arterial Tortuosity," Arterioscler., Thromb., Vasc. Biol., **25**(5), pp. 957–962.
[36] Lawrence, A. R., and Gooch, K. J., 2009, "Transmural Pressure and Axial Loading Interactively Regulate Arterial Remodeling Ex Vivo," Am. J. Physiol.: Heart Circ. Physiol., **297**(1), pp. H475–H484.
[37] Cocciolone, A. J., Hawes, J. Z., Staiculescu, M. C., Johnson, E. O., Murshed, M., and Wagenseil, J. E., 2018, "Elastin, Arterial Mechanics, and Cardiovascular Disease," Am. J. Physiol.: Heart Circ. Physiol., **315**(2), pp. H189–H205.
[38] Bersi, M. R., Khosravi, R., Wujciak, A. J., Harrison, D. G., and Humphrey, J. D., 2017, "Differential Cell-Matrix Mechanoadaptations and Inflammation Drive Regional Propensities to Aortic Fibrosis, Aneurysm or Dissection in Hypertension," J. R. Soc. Interface, **14**(136), p. 20170327.